Supporting information

Simultaneous improvement of power factor and thermal conductivity via Ag doping in p-type Mg_3Sb_2 thermoelectric materials

Lirong Song,‡ Jiawei Zhang,‡ and Bo B. Iversen*

Center for Materials Crystallography, Department of Chemistry and iNANO, Aarhus University, Langelandsgade 140, Aarhus DK-8000, Denmark.

*E-mail: bo@chem.au.dk

‡ These authors contribute equally.

Calculation details of electronic transport

Electrical transport properties in the main text are simulated using combined full band structure calculation and semiclassical Boltzmann transport theory under the constant scattering time approximation (CSTA) in BoltzTraP code.[1] Under the CSTA, it is assumed that the carrier scattering time τ remains constant with varying temperature and doping level. The simulated Seebeck coefficient is independent of τ, while electrical conductivity and power factor are calculated with respect to the constant carrier scattering time τ. This approach has been successfully applied in the prediction of Seebeck coefficient values and the trends of electrical conductivity and power factor of a wide range of thermoelectric materials.[2-6]

In addition to CSTA, the single parabolic band model is also used in the main text. Under a single parabolic band approximation, the Seebeck coefficient and the Lorenz number can be written as[7]

$$S = -\frac{k_B}{e}\left(\eta - \frac{\left(r+\frac{5}{2}\right)F_{r+3/2}(\eta)}{\left(r+\frac{3}{2}\right)F_{r+1/2}(\eta)}\right) \quad (1)$$

$$L = \left(\frac{k_B}{e}\right)^2 \left\{\frac{\left(r+\frac{7}{2}\right)F_{r+5/2}(\eta)}{\left(r+\frac{3}{2}\right)F_{r+1/2}(\eta)} - \left[\frac{\left(r+\frac{5}{2}\right)F_{r+3/2}(\eta)}{\left(r+\frac{3}{2}\right)F_{r+1/2}(\eta)}\right]^2\right\} \quad (2)$$

where Fermi integral is

$$F_n(\eta) = \int_0^\infty \frac{\varepsilon^n d\varepsilon}{1+\exp(\varepsilon-\eta)}, \quad (3)$$

k_B is the Boltzmann constant, h is the Planck's constant, η is the reduced Fermi energy. Scattering factor r = -0.5 is assumed for the acoustic phonon scattering mechanism.

The average zT shown in Figure 8b in the main text was calculated by the following formula:[8]

$$zT_{avg} = \frac{\left(\int_{T_c}^{T_h} S(T)dT\right)^2 (T_h - T_c)}{\left(\int_{T_c}^{T_h} \rho(T)dT\right)\left(\int_{T_c}^{T_h} \kappa(T)dT\right)}, \quad (4)$$

where T_h and T_c are temperatures of the hot side and the cold side, respectively. In Figure 8b, T_c was chosen to be 333 K since the reported thermoelectric properties of $Mg_3Sb_{1.8}Bi_{0.2}$ (ref. 9) were measured from 333 K.

Table S1. The nominal and actual compositions measured by SEM-EDS for $Mg_{3-x}Ag_xSb_2$ ($0 \le x \le 0.025$) samples, It should be noted that the actual compositions of Ag by SEM-EDS have large errors due to the small amount of Ag doping.

$Mg_{3-x}Ag_xSb_2$	Nominal compositions	Actual compositions (SEM-EDS)	Intensity Error (%)		
			MgK	AgL	SbL
x = 0	$Mg_{60}Sb_{40}$	$Mg_{52.89}Sb_{47.11}$	0.80	-	0.50
x = 0.005	$Mg_{59.9}Ag_{0.1}Sb_{40}$	$Mg_{51.06}Ag_{0.49}Sb_{48.45}$	0.91	13.89	0.54
x = 0.01	$Mg_{59.8}Ag_{0.2}Sb_{40}$	$Mg_{50.94}Ag_{0.47}Sb_{48.59}$	0.89	14.90	0.54
x = 0.015	$Mg_{59.7}Ag_{0.3}Sb_{40}$	$Mg_{50.68}Ag_{0.76}Sb_{48.56}$	0.91	9.59	0.55
x = 0.02	$Mg_{59.6}Ag_{0.4}Sb_{40}$	$Mg_{51.73}Ag_{0.52}Sb_{47.75}$	0.84	13.47	0.52
x = 0.025	$Mg_{59.5}Ag_{0.5}Sb_{40}$	$Mg_{51.51}Ag_{0.76}Sb_{47.73}$	0.85	9.05	0.53

Table S2. The sample densities, theoretical densities and relative densities of $Mg_{3-x}Ag_xSb_2$ ($0 \le x \le 0.025$) samples. The relative densities of all the samples are larger than 96%.

$Mg_{3-x}Ag_xSb_2$	Sample density (g/cm^3)	Theoretical density (g/cm^3)	Relative density (%)
x = 0	3.891	4.013	97.0
x = 0.005	3.881	4.006	96.9
x = 0.01	3.913	4.010	97.6
x = 0.015	3.865	4.014	96.3
x = 0.02	3.892	4.026	96.7
x = 0.025	3.932	4.029	97.6

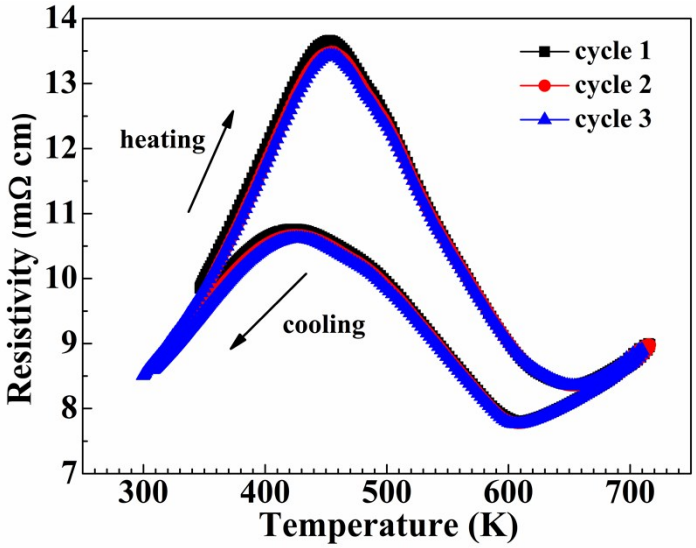

Fig. S1. Repeated measurements of electrical resistivity in the last 3 cycles for $Mg_{3-x}Ag_xSb_2$ (x=0.015), showing the sample is stable during the measurements.

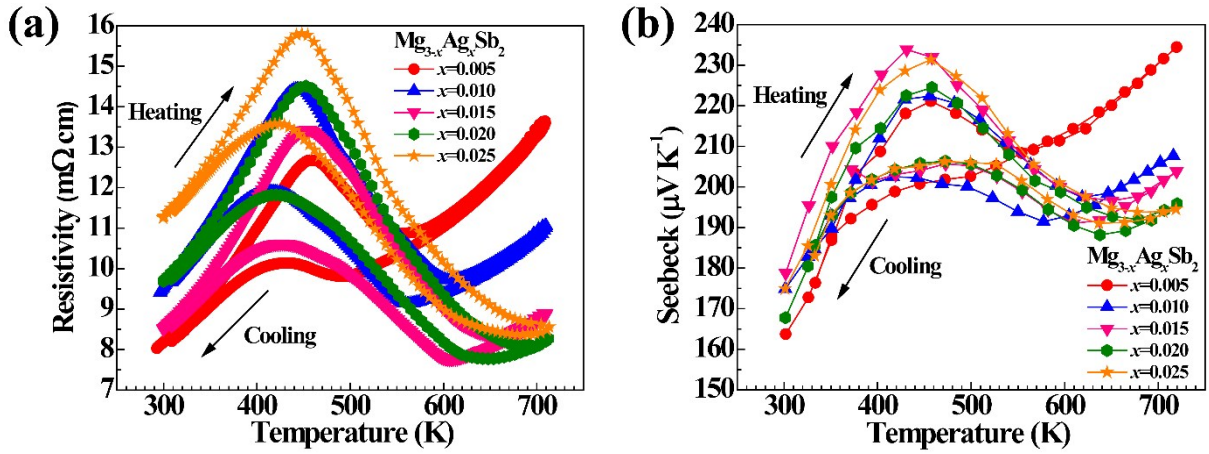

Fig. S2. Electrical resistivity (a) and Seebeck coefficient (b) of $Mg_{3-x}Ag_xSb_2$ ($0.005 \le x \le 0.025$) samples with both heating and cooling measurements of the final cycle.

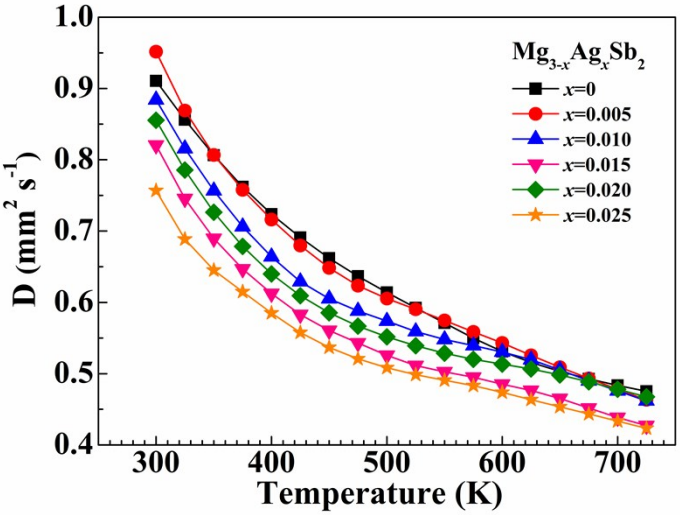

Fig. S3. Temperature dependence of thermal diffusivity of $Mg_{3-x}Ag_xSb_2$ ($0 \le x \le 0.025$).

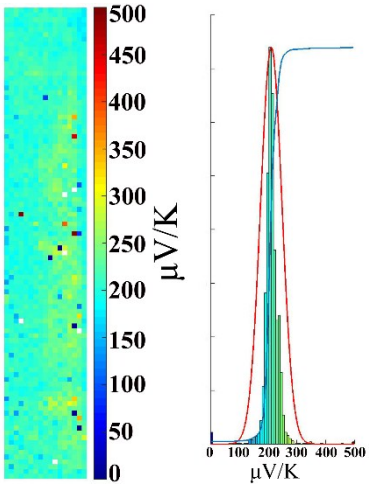

Fig. S4. Scanning Seebeck coefficient map and histogram over the cross section of $Mg_{3-x}Ag_xSb_2$ (x=0.015) pellet.

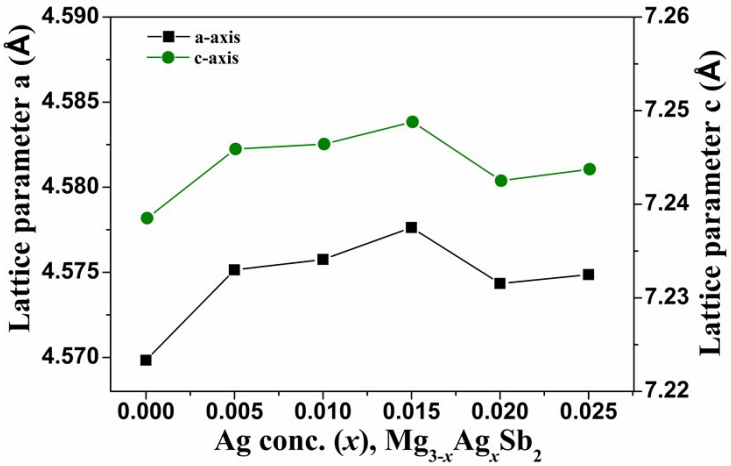

Fig. S5. Lattice parameters as a function of the Ag doping content in $Mg_{3-x}Ag_xSb_2$ ($0 \le x \le 0.025$). The lattice parameters are estimated by the Rietveld refinement using the Fullprof program.[10]

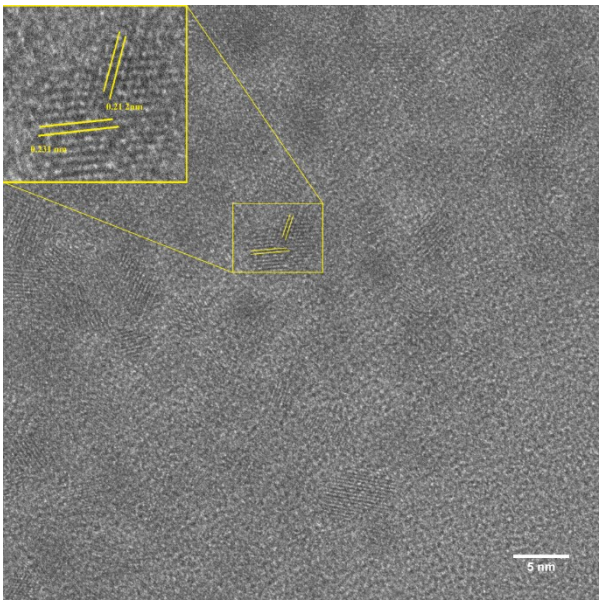

Fig. S6. The atomic-scale high resolution TEM image of the undoped sample, exihibiting the presence of different orientations of the crystallographic planes: 110 (0.231 nm) and 103 (0.212 nm).

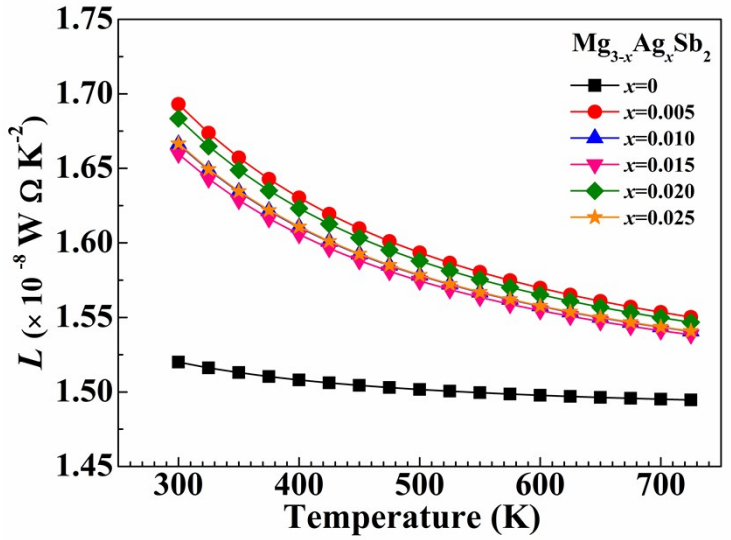

Fig. S7. Temperature dependence of the Lorenz numbers of $Mg_{3-x}Ag_xSb_2$ ($0 \le x \le 0.025$) estimated by the single parabolic band model.

References

(1) G. K. H. Madsen, D. J. Singh, *Comput. Phys. Commun.* 2006, **175**, 67-71.
(2) G. K. H. Madsen, *J. Am. Chem. Soc.* 2006, **128**, 12140-12146.
(3) J. Yang, H. Li, T. Wu, W. Zhang, L. Chen, J. Yang, *Adv. Funct. Mater.* 2008, **18**, 2880-2888.
(4) J. Zhang, L. Song, G. K. H. Madsen, K. F. F. Fischer, W. Zhang, X. Shi, B. B. Iversen, *Nat. Commun.* 2016, **7**, 10892.
(5) J. Zhang, R. Liu, N. Cheng, Y. Zhang, J. Yang, C. Uher, X. Shi, L. Chen, W. Zhang, *Adv. Mater.* 2014, **26**, 3848-3853.
(6) D. J. Singh, D. Parker, *J. Appl. Phys.* 2013, **114**, 143703.
(7) H. J. Goldsmid, *Thermoelectric Refrigeration*; Plenum Press: New York, 1964.
(8) H. S. Kim, W. Liu, G. Chen, C.W. Chu, Z. Ren, *Proc. Natl. Acad. Sci. U.S.A.* 2015, **112**, 8205-8210.
(9) A. Bhardwaj, A. Rajput, A. K. Shukla, J. J. Pulikkotil, A. K. Srivastava, A. Dhar, G. Gupta, S. Auluck, D. K. Misra, R. C. Budhani, *RSC Adv.* 2013, **3**, 8504-8516.
(10) J. Rodríguez-Carvajal, *Physica B* 1993, **192**, 55-69.